Journal of Computational Physics 371 (2018) 850–869

Contents lists available at ScienceDirect

Journal of Computational Physics

www.elsevier.com/locate/jcp

An upwind CESE scheme for 2D and 3D MHD numerical simulation in general curvilinear coordinates

Yun Yang [a,b,*], Xue-Shang Feng [a,c,*], Chao-Wei Jiang [c,a]

[a] SIGMA Weather Group, State Key Laboratory of Space Weather, National Space Science Center, CAS, Beijing, China
[b] University of Chinese Academy of Sciences, Beijing, China
[c] Institute of Space Science and Applied Technology, Harbin Institute of Technology, Shenzhen, China

ARTICLE INFO

Article history:
Received 29 October 2017
Received in revised form 26 April 2018
Accepted 7 May 2018
Available online 16 May 2018

Keywords:
Upwind
CESE scheme
MHD
Curvilinear coordinates
Transforming
Divergence-free

ABSTRACT

Shen et al. [1,2] proposed an upwind space-time conservation element and solution element (CESE) scheme for 1D and 2D hydrodynamics (HD) in rectangular coordinates, which combined the advantages of CESE and upwind scheme, namely, guaranteed strictly the space–time conservation law as well as captured discontinuities very efficiently. All kinds of upwind schemes can be combined very flexibly for different problems to achieve the perfect combination of CESE and finite volume method (FVM). However, in many physical applications, we need to consider geometries that are more sophisticated. Hence, the main objective of this paper is to extend the upwind CESE scheme to multidimensional magneto-hydrodynamics (MHD) in general curvilinear coordinates by transforming the MHD equations from the physical domain (general curvilinear coordinates) to the computational domain (rectangular coordinates) and the new equations in the computational domain can be still written in the conservation form. For the 3D case, the derivations of some formulas are much more abstract and complex in a 4D Euclidean hyperspace, and some technical problems need to be solved in the debugging process. Unlike in HD, keeping the magnetic field divergence-free for MHD problems is also a challenge especially in general curvilinear coordinates. These are the main obstacles we have overcome in this study. The test results of benchmarks demonstrate that we have successfully extended the upwind CESE scheme to general curvilinear coordinates for both 2D and 3D MHD problems.

1. Introduction

Some complex flow phenomena such as shock and other discontinuities as well as shear layers are often met with for HD and MHD problems. Many researchers have tried their best to design schemes which can maximize accuracy and robustness in dealing with complex flow problems. Upwind schemes are most popular in dealing with discontinuous problems, and these can be split into three groups [3,4]: flux vector splitting (FVS), flux difference splitting (FDS) and CUSP family (including AUSM [5,6], CUSP [7–11], LDFSS [12], AUFS [13]). In fact, CUSP family are special FVS schemes. The usually used FVS schemes mainly include three types for HD [4]: Steger–Warming [14], Lax–Friedrichs [15], and Van-Leer [16] splitting. MacCormack [17] developed an FVS method for MHD to overcome the challenge of inhomogeneous coefficient matrices of MHD equations. The usually used FDS schemes mainly include HLL [18–21], HLLC [20,22–25], HLLD [26,27], Roe [23,28,29]

* Corresponding authors at: National Space Science Center, University of Chinese Academy of Sciences, Beijing, China.
E-mail addresses: yangyun@spaceweather.ac.cn (Y. Yang), fengx@spaceweather.ac.cn (X.-S. Feng).

https://doi.org/10.1016/j.jcp.2018.05.014
0021-9991/

and one TVD scheme proposed by Balsara [30] which is based on a linearized formulation of the Riemann problem [31,32]. Later, some new hybrid schemes were developed, combining two or more isolated schemes to obtain a better scheme than just using any one of these schemes. Up to now, we have known mainly three types of hybrid schemes: Hybrid flux-splitting schemes [33–38]; PISO + AUSM [39,40]; Rotated Riemann solver [41–43]. The hybrid flux-splitting schemes are those trying to combine the accuracy of FDS and the robustness of FVS in dealing with problems including discontinuities. The basic idea of hybrid flux-splitting scheme is to first split the flux by FVS, and then for each split parts use an appropriate FDS scheme. PISO + AUSM is a scheme in which after splitting the flux by AUSM, the PISO cycle method is used to predict and correct the states variables. Rotated Riemann solvers split the local normal vectors at each solution point into two normal vectors. Then, they treat the direction with discontinuities by using a highly diffusive scheme. The other direction, which is more continuous, is treated with a lower diffusion scheme to get a more accurate solution in the smooth direction. The aim is to get a more accurate and robust scheme to handle the problems of discontinuities.

The CESE scheme was first proposed by Chang [44], to be developed for and applied to HD successfully. The main characteristic of the CESE scheme is that it deals with space and time as one entity when discretizing conservation equations which can strongly guarantee the space-time conservation law. Besides, it also has some other attractive advantages over the FVM [45]. But it didn't consider the eigen-structures [2]. We have found from the tests that: for the original CESE scheme, though some artificial dissipation had been embedded into the scheme in the process of derivation of first-order derivative, some discontinuous surfaces have been smeared out more or less. By analyzing Fourier stability and accuracy properties, Huynh [46] pointed out that upwind scheme is more accurate than the original CESE scheme on quadrilateral meshes. To combine the advantages of the CESE scheme and upwind scheme together, Shen et al. [1,2] proposed an upwind CESE scheme for 1D and 2D HD on rectangular grids, which can capture discontinuities very well.

Some practical MHD problems such as solar-terrestrial physics problems, the sun's and earth's geometry (spherical shaped) will need spherical coordinates. Shocks and other discontinuities, such as contact discontinuity, tangential discontinuity, rotational discontinuity are often encountered in many space physics events. These problems motivate us to study and construct an upwind CESE scheme in general curvilinear coordinates by transforming the MHD equations from the physical domain (general curvilinear coordinates) to the computational domain (rectangular coordinates) which won't change the conservation property of governing equations [47,48].

The remainder of this paper is organized as follows. The MHD governing equations are presented in Section 2. Section 3 presents the construction of the 2D and 3D upwind CESE scheme in rectangular coordinates and general curvilinear coordinates, respectively. Section 4 gives a method to clean magnetic field divergence by using the least-squares method. Some standard benchmarks are used in Section 5 to check the effectiveness of this upwind scheme for the 2D and 3D MHD problems in both rectangular coordinates and general curvilinear coordinates. Section 6 presents the conclusions.

2. MHD governing equations

The ideal MHD equations in conservative form in physical domain are as follows:

$$\frac{\partial \mathbf{U}}{\partial t} + \nabla \cdot \widehat{\mathbf{F}} = 0, \tag{1}$$

where $\mathbf{U} = (u_m) = (\rho, \rho v_x, \rho v_y, \rho v_z, E, B_x, B_y, B_z)^{\mathrm{T}}$ is the state vector of conservative variables and $m = 1, \ldots, 8$. t, γ, ρ, E, $\mathbf{V} = (v_x, v_y, v_z)$ and $\mathbf{B} = (B_x, B_y, B_z)$ denote time, the ratio of specific heats, the mass density, total energy, plasma velocity and magnetic field, respectively.

$p = (\gamma - 1)(E - \frac{\mathbf{V}\cdot\mathbf{V}}{2} - \frac{\mathbf{B}\cdot\mathbf{B}}{2})$ is the gas pressure and $p_0 = p + \frac{\mathbf{B}\cdot\mathbf{B}}{2}$ is the total pressure. $\widehat{\mathbf{F}}$ denotes the flux vector, which equals $\mathbf{F}$, $(\mathbf{F}, \mathbf{G})$ and $(\mathbf{F}, \mathbf{G}, \mathbf{H})$ for 1, 2 and 3 dimensions, respectively. And

$$\begin{aligned}
\mathbf{F} = (f_m) = \big[&\rho v_x, \rho v_x^2 + p_0 - B_x^2, \rho v_x v_y - B_x B_y, \rho v_x v_z - B_x B_z, (E + p) v_x - B_x(\mathbf{V}\cdot\mathbf{B}), 0, v_x B_y \\
&- v_y B_x, v_x B_z - v_z B_x\big]^{\mathrm{T}}, \\
\mathbf{G} = (g_m) = \big[&\rho v_y, \rho v_y v_x - B_y B_x, \rho v_y^2 + p_0 - B_y^2, \rho v_y v_z - B_y B_z, (E + p) v_y - B_y(\mathbf{V}\cdot\mathbf{B}), v_y B_x \\
&- v_x B_y, 0, v_y B_z - v_z B_y\big]^{\mathrm{T}}, \\
\mathbf{H} = (h_m) = \big[&\rho v_z, \rho v_z v_x - B_z B_x, \rho v_z v_y - B_z B_y, \rho v_z^2 + p_0 - B_z^2, (E + p) v_z - B_z(\mathbf{V}\cdot\mathbf{B}), v_z B_x \\
&- v_x B_z, v_z B_y - v_y B_z, 0\big]^{\mathrm{T}}.
\end{aligned}$$

3. Construction of upwind CESE scheme

3.1. Upwind CESE scheme in rectangular coordinates for the 2D case

In the generalized 3D Euclidean space $E_{2+1}(x, y, t)$, which combines the spatial coordinates with time t, Eq. (1) can be rewritten as follows:

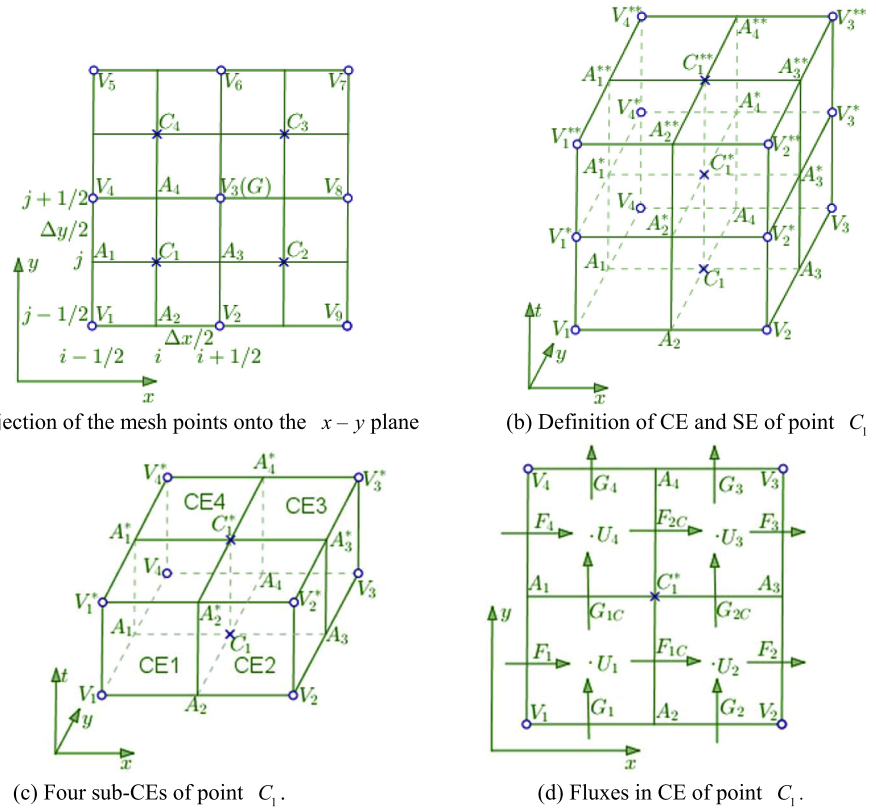

Fig. 1. (a) spatial meshes; (b) definition of CE and SE; (c) one CE split into four sub-CEs; (d) corresponding fluxes in the upwind CESE scheme on rectangular meshes.

$$\nabla \cdot \mathbf{h}_m = 0, \tag{2}$$

where $\mathbf{h}_m = (f_m, g_m, u_m)$, $(m = 1, \ldots, 8)$ is the space-time flux vector. By applying Gauss's divergence theorem into Eq. (2) in the 3D space-time domain $E_{2+1}(x, y, t)$, we obtain

$$\oint_{S(V)} \mathbf{h}_m \cdot \mathrm{d}\mathbf{s} = 0, \tag{3}$$

where $S(V)$ is the boundary of any closed space-time region V in $E_{2+1}(x, y, t)$.

$\mathrm{d}\mathbf{s} = (\mathrm{d}\delta)\mathbf{n}$, $\mathrm{d}\delta$ and $\mathbf{n}$ are the area and unit outward normal vector of a surface element on $S(V)$, respectively. $\mathbf{h}_m \cdot \mathrm{d}\mathbf{s}$ denotes the total space-time flux leaving the surface element $\mathrm{d}\mathbf{s}$.

As Fig. 1(a) shows, the space-time domain is discretized by a uniform mesh in rectangular coordinates. V_i denotes the i-th vertex point, and A_i denotes the i-th mid-point of the element edge. As reported earlier [49], for quadrilateral cells, each cell is associated with four basic conservation elements (BCEs), which constitute a compound CE (CCE). In Fig. 1(a), $V_1V_5V_7V_9$ is the projection of one CCE, and the projections of four BCEs related to it are $(V_1V_2V_3V_4)$, $(V_3V_4V_5V_6)$, $(V_6V_7V_8V_3)$ and $(V_8V_3V_2V_9)$. C_i is the centroid of the i-th BCE. G is the centroid of CCE. C_i and G are also the solution points of the BCEs and CCE, respectively.

Uniformity of the meshes makes the centroids coincide with the centers of quadrilaterals. The final solution point G coincides with the vertex point V_3.

There are mainly two kinds of CESE schemes: non-staggered and staggered [2]. In this study, we use the staggered one, mainly because it can save memory and reduce computational cost. In a full time step, during the first half time step, the solution is updated from the vertices marked by hollow circles to the respective cell centers marked by crosses in Fig. 1(a). During the second half time step, the solution is updated from the cell centers to the vertices.

To be more specific, for a cell point, we first update the solution of its four BCEs, namely C_i, during the first half time step. Following which the values of C_i are used to update the solution of the CCE, namely G, during the second half time step.

For each set of solution points C_i and G, we define a conservation element (CE) and a corresponding solution element (SE). For the upwind CESE scheme, the CE is the same as in the original CESE scheme but the SE is different from the original one. Below, we take the point C_1^* as an example. As Fig. 1(b) shows, CE (C_1^*) is the hexahedron $V_1V_2V_3V_4V_1^*V_2^*V_3^*V_4^*$; in

the original CESE scheme, its corresponding SE(C_1^*) is the union of three planes $V_1^*V_2^*V_3^*V_4^*$, $A_1A_3A_3^{**}A_1^{**}$ and $A_2A_4A_4^{**}A_2^{**}$, which are orthogonal to each other and intersect at C_1^*. In the upwind CESE scheme, corresponding SE (C_1^*) is the union of planes $A_1A_3A_3^*A_1^*$, $A_2A_4A_4^*A_2^*$ and hexahedron $V_1^*V_2^*V_3^*V_4^*V_1^{**}V_2^{**}V_3^{**}V_4^{**}$. Let Ψ, Ψ^* and Ψ^{**} denote any point at $n-1/2$ time level, n time level and $n+1/2$ time level, where n is the index for time.

As the conservation law, i.e., Eq. (3), is suitable for an arbitrary closed space-time domain, the CE we constructed in Fig. 1(b) will facilitate the derivation of the discrete form of Eq. (3). All the boundaries of the CEs are parallel to the coordinate surfaces, and the normal direction is along the coordinate axis; therefore, on any boundary surface of CEs, there is only one component of the total space-time fluxes, which makes the integration of space-time fluxes much more convenient.

Inside SE(Ψ) of any point Ψ, all the space-time fluxes u_m, f_m and g_m are approximated by Taylor expansion at point Ψ. Each CE can be split into four sub-CEs; for example, CE (C_1) can be split into CE1, CE2, CE3 and CE4 as shown in Fig. 1(c). Imposing conservation law, i.e., Eq. (3), on each sub-CE, we get

$$\begin{aligned} U_1^*(C_1^*)\frac{\Delta x\Delta y}{4} &= \left[u_m(C_1^*) - u_{mx}(C_1^*)\frac{\Delta x}{4} - u_{my}(C_1^*)\frac{\Delta y}{4}\right]\frac{\Delta x\Delta y}{4} \\ &= U_1\frac{\Delta x\Delta y}{4} + (F_1 - F_{1C})\frac{\Delta y\Delta t}{4} + (G_1 - G_{1C})\frac{\Delta x\Delta t}{4}, \end{aligned} \tag{4}$$

$$\begin{aligned} U_2^*(C_1^*)\frac{\Delta x\Delta y}{4} &= \left[u_m(C_1^*) + u_{mx}(C_1^*)\frac{\Delta x}{4} - u_{my}(C_1^*)\frac{\Delta y}{4}\right]\frac{\Delta x\Delta y}{4} \\ &= U_2\frac{\Delta x\Delta y}{4} + (F_{1C} - F_2)\frac{\Delta y\Delta t}{4} + (G_2 - G_{2C})\frac{\Delta x\Delta t}{4}, \end{aligned} \tag{5}$$

$$\begin{aligned} U_3^*(C_1^*)\frac{\Delta x\Delta y}{4} &= \left[u_m(C_1^*) + u_{mx}(C_1^*)\frac{\Delta x}{4} + u_{my}(C_1^*)\frac{\Delta y}{4}\right]\frac{\Delta x\Delta y}{4} \\ &= U_3\frac{\Delta x\Delta y}{4} + (F_{2C} - F_3)\frac{\Delta y\Delta t}{4} + (G_{2C} - G_3)\frac{\Delta x\Delta t}{4}, \end{aligned} \tag{6}$$

$$\begin{aligned} U_4^*(C_1^*)\frac{\Delta x\Delta y}{4} &= \left[u_m(C_1^*) - u_{mx}(C_1^*)\frac{\Delta x}{4} + u_{my}(C_1^*)\frac{\Delta y}{4}\right]\frac{\Delta x\Delta y}{4} \\ &= U_4\frac{\Delta x\Delta y}{4} + (F_4 - F_{2C})\frac{\Delta y\Delta t}{4} + (G_{1C} - G_4)\frac{\Delta x\Delta t}{4}, \end{aligned} \tag{7}$$

where U_i and F_i, G_i represent the conservative variables and original interface fluxes of sub-CEs which can be obtained by Taylor expansion from the point V_i. F_{jC} and G_{jC} denote the newly adding upwind interface fluxes as shown in Fig. 1(d), which can be obtained by solving Riemann solver and any upwind schemes can be used.

$$U_i = u_m(V_i) + \frac{k_x\Delta x}{4}u_{mx}(V_i) + \frac{k_y\Delta y}{4}u_{my}(V_i), \tag{8}$$

$$F_i = f_m(V_i) + \frac{k_y\Delta y}{4}f_{my}(V_i) + \frac{\Delta t}{4}f_{mt}(V_i), \tag{9}$$

$$G_i = g_m(V_i) + \frac{k_x\Delta x}{4}g_{mx}(V_i) + \frac{\Delta t}{4}g_{mt}(V_i), \tag{10}$$

$$F_{jc}/G_{jc} = \Phi\left(u_{mL}^{n-1/4}, u_{mR}^{n-1/4}\right), \tag{11}$$

where k_x, k_y is -1 or 1, as determined by the position of the four solution points V_1, V_2, V_3, V_4 relative to the center point C_1, and they are $(-1,-1), (1,-1), (1,1), (-1,1)$, respectively. We used the chain rule to obtain $f_{mt}(V_i)$ and $g_{mt}(V_i)$, for example, $f_{mt}(V_i) = \frac{\partial f_m(V_i)}{\partial t} = \sum_{p=1}^{8}\frac{\partial f_m(V_i)}{\partial u_p(V_i)}u_{pt}(V_i)$, where $u_{pt}(V_i) = -f_{px}(V_i) - g_{py}(V_i)$ which was obtained according to the conservation law expressed by Eq. (1). $\Phi(u_{mL}^{n-1/4}, u_{mR}^{n-1/4})$ can be obtained by any upwind scheme, such as HLL, HLLC, HLLD, Roe or some hybrid FVS and FDS schemes.

Adding Eqs. (4)–(7) together, we obtain

$$u_m(C_1^*) = \frac{1}{4}(U_1 + U_2 + U_3 + U_4) + \frac{\Delta t}{4\Delta x}(F_1 - F_2 - F_3 + F_4) + \frac{\Delta t}{4\Delta y}(G_1 + G_2 - G_3 - G_4). \tag{12}$$

Subtracting Eq. (4) from Eq. (5) and subtracting Eq. (7) from Eq. (6), we obtain two groups of u_{mx}

$$u_{mx}(C_1^*) = \frac{2}{\Delta x}\left[(U_2 - U_1) + \frac{\Delta t}{\Delta x}(2F_{1C} - F_1 - F_2) + \frac{\Delta t}{\Delta y}(G_2 - G_1 + G_{1C} - G_{2C})\right], \tag{13}$$

$$u_{mx}(C_1^*) = \frac{2}{\Delta x}\left[(U_3 - U_4) + \frac{\Delta t}{\Delta x}(2F_{2C} - F_3 - F_4) + \frac{\Delta t}{\Delta y}(G_4 - G_3 + G_{2C} - G_{1C})\right]. \tag{14}$$

Subtracting Eq. (4) from Eq. (7) and subtracting Eq. (5) from Eq. (6), we obtain two groups of u_{my}

$$u_{my}(C_1^*) = \frac{2}{\Delta y}\left[(U_3 - U_2) + \frac{\Delta t}{\Delta x}(F_2 - F_3 + F_{2C} - F_{1C}) + \frac{\Delta t}{\Delta y}(2G_{2C} - G_2 - G_3)\right], \tag{15}$$

$$u_{my}(C_1^*) = \frac{2}{\Delta y}\left[(U_4 - U_1) + \frac{\Delta t}{\Delta x}(F_4 - F_1 + F_{1C} - F_{2C}) + \frac{\Delta t}{\Delta y}(2G_{1C} - G_1 - G_4)\right]. \tag{16}$$

Then, by directly using the arithmetic average or by using a weighted average function [50,51], the final values of u_{mx} and u_{my} can be obtained for the HD problems. However, for the MHD, to control the magnetic field divergence-free, we will use least-squares method to obtain the first-order derivatives of B_x, B_y and B_z which will be discussed in Section 4.

In fact, you can find that Eq. (12) is the same as the original CESE scheme in the process of updating u_m. The center interface upwind fluxes only play a part in updating the first-order derivatives of the conservative variables.

3.2. Upwind CESE scheme in general curvilinear coordinates for the 2D case

By using a nonsingular mapping $x = x(\xi, \eta)$; $y = y(\xi, \eta)$, Eq. (1) can be transformed from the physical domain (x, y) to a computational domain (ξ, η). $\mathbf{J} = \frac{\partial(x,y)}{\partial(\xi,\eta)} = \begin{pmatrix} x_\xi & x_\eta \\ y_\xi & y_\eta \end{pmatrix}$ is the Jacobian matrix and its components are called metrics which can be calculated numerically or analytically. The inverse matrix of the Jacobian matrix is $\mathbf{J}^{-1} = \frac{\partial(\xi,\eta)}{\partial(x,y)} = \begin{pmatrix} \xi_x & \xi_y \\ \eta_x & \eta_y \end{pmatrix}$. Here, we use the mapping $x = e^\xi \cos\eta$, $y = e^\xi \sin\eta$. Thus, the Jacobian matrix can be obtained analytically. In the following text, if there is no special explanation, all the quantities in computational domain will be labeled by "$\sim$".

After transformation, the 2D ideal MHD equations in computational domain are as follows:

$$\frac{\partial \widetilde{\mathbf{U}}}{\partial t} + \frac{\partial \widetilde{\mathbf{F}}}{\partial \xi} + \frac{\partial \widetilde{\mathbf{G}}}{\partial \eta} = 0, \tag{17}$$

where

$$\begin{aligned} \widetilde{\mathbf{U}} &= J\mathbf{U}, \\ \widetilde{\mathbf{F}} &= J\xi_x\mathbf{F} + J\xi_y\mathbf{G}, \\ \widetilde{\mathbf{G}} &= J\eta_x\mathbf{F} + J\eta_y\mathbf{G}, \end{aligned} \tag{18}$$

and J is the determinant of the Jacobian.

Vinokur [47] and Viviand [48] reported that using transformation wouldn't change the conservation property of equations, so the conservation law is satisfied in the computational domain. Eq. (17) can be rewritten in conservative form as:

$$\nabla \cdot \widetilde{\mathbf{h}} = 0, \tag{19}$$

where $\widetilde{\mathbf{h}} = (\widetilde{\mathbf{F}}, \widetilde{\mathbf{G}}, \widetilde{\mathbf{U}})$.

In the 3D Euclidean space $E_{2+1}(\xi, \eta, t)$, by applying Gauss's divergence theorem into Eq. (17), we obtain

$$\oint_{S(V)} \widetilde{\mathbf{h}} \cdot d\mathbf{s} = 0. \tag{20}$$

As Fig. 3(b) shows, in the computational domain, they are rectangular grids, so the method in Section 3.1 can be built in the computational domain in a similar manner. We should note that, in the computational domain, the independent marching variables are $\widetilde{\mathbf{U}}, \widetilde{\mathbf{U}}_\xi, \widetilde{\mathbf{U}}_\eta$. When using Taylor expansions for flux vectors, we also need to get the derivatives of flux vectors in the computational domain. By taking the derivative of Eq. (18) with respect to ξ or η, we obtain the relationships of conservative variables and flux vectors as well as their corresponding spatial derivatives in the physical domain and computational domain are as follows:

$$\begin{aligned} &\widetilde{\mathbf{U}}_\phi = J_\phi\mathbf{U} + J\mathbf{U}_\phi, \\ &\widetilde{\mathbf{F}}_\phi = (J\xi_x)_\phi\mathbf{F} + (J\xi_y)_\phi\mathbf{G} + J\xi_x\mathbf{F}_\phi + J\xi_y\mathbf{G}_\phi, \\ &\widetilde{\mathbf{G}}_\phi = (J\eta_x)_\phi\mathbf{F} + (J\eta_y)_\phi\mathbf{G} + J\eta_x\mathbf{F}_\phi + J\eta_y\mathbf{G}_\phi, \\ &\mathbf{U}_\phi = \mathbf{U}_x x_\phi + \mathbf{U}_y y_\phi, \qquad \mathbf{F}_\phi = \frac{\partial \mathbf{F}}{\partial \mathbf{U}}\mathbf{U}_\phi, \qquad \mathbf{G}_\phi = \frac{\partial \mathbf{G}}{\partial \mathbf{U}}\mathbf{U}_\phi, \end{aligned} \tag{21}$$

where the subscript "ϕ" denotes ξ or η. $\frac{\partial \mathbf{F}}{\partial \mathbf{U}}$, $\frac{\partial \mathbf{G}}{\partial \mathbf{U}}$ are the Jacobian matrices for fluxes in the physical domain. J_ϕ, $J\xi_x$, $J\xi_y$, $J\eta_x$, $J\eta_y$, $(J\xi_x)_\phi$, $(J\xi_y)_\phi$, $(J\eta_x)_\phi$ and $(J\eta_y)_\phi$ all can be obtained analytically according to the mapping relation.

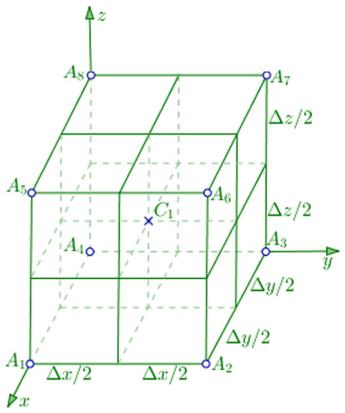

Fig. 2. Projection of the mesh points in E_{3+1} onto the x–y–z plane.

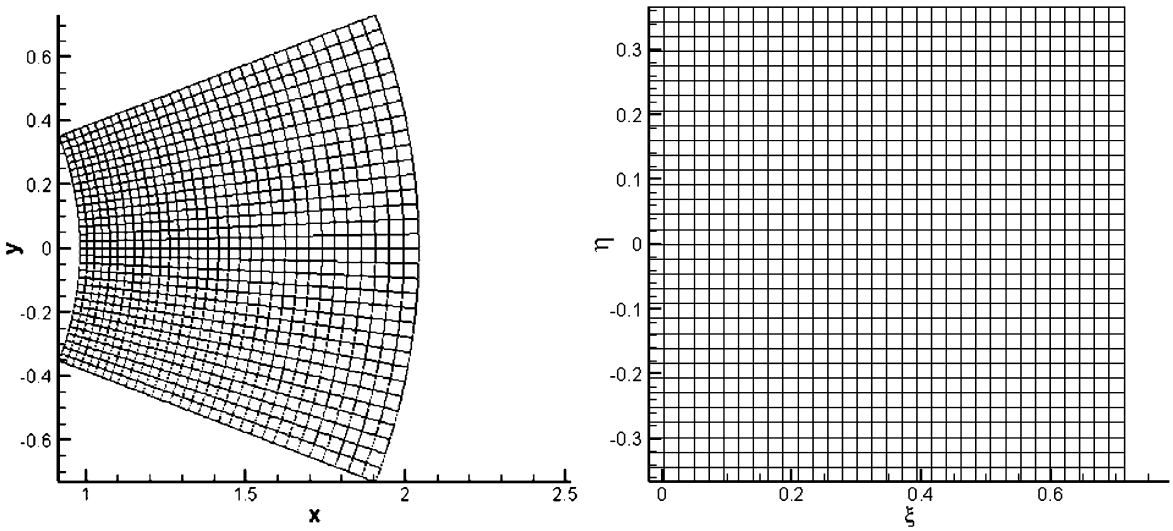

(a) Physical domain (b) Computational domain

Fig. 3. (a) Physical domain and (b) computational domain for the 2D case.

After updating variables in the computational domain, we need to use inverse transformation to get the variables in the physical domain, the relevant inverse transformations are as follows:

$$\mathbf{U} = \widetilde{\mathbf{U}}/J,$$
$$\mathbf{U}_\xi = (\widetilde{\mathbf{U}}_\xi - J_\xi \mathbf{U})/J,$$
$$\mathbf{U}_\eta = (\widetilde{\mathbf{U}}_\eta - J_\eta \mathbf{U})/J,$$
$$\mathbf{U}_x = \mathbf{U}_\xi \xi_x + \mathbf{U}_\eta \eta_x,$$
$$\mathbf{U}_y = \mathbf{U}_\xi \xi_y + \mathbf{U}_\eta \eta_y.$$

Below we will give a special introduction about the calculation of upwind fluxes, take the $\widetilde{F}_{1C}$ as an example. Firstly, in the computational domain, Taylor expansion is used to get the left and right values $\widetilde{\mathbf{U}}_L, \widetilde{\mathbf{U}}_R$ from points V_1 and V_2, respectively. Then, transformation is used to get the left and right values $\mathbf{U}_L, \mathbf{U}_R$ as well as the fluxes $\mathbf{F}_L, \mathbf{F}_R, \mathbf{G}_L, \mathbf{G}_R$ in the physical domain. Finally, fluxes in the computational domain are obtained by using the second equality of Eq. (18).

3.3. Upwind CESE scheme in rectangular coordinates and general curvilinear coordinates for the 3D case

For the 3D case, the grid is split as shown in Fig. 2; it's defined in a 4D hyperspace, some figures we can't give visually, only through imagination. Such as the SE(C_1^*) of point C_1^* is defined as the union of four hyperplanes x–y–z, x–y–t, x–z–t and y–z–t, which intersect at C_1^*. Moreover, the corresponding CE(C_1^*) is formed by hypersurfaces associated with SE (C_1^*),

SE (A_1), SE (A_2), SE (A_3), SE (A_4), SE (A_5), SE (A_6), SE (A_7) and SE (A_8). In analogy with the 2D case, each CE can be split into eight sub-CEs, and by imposing conservation law, i.e., Eq. (3) on each sub-CE, we can get u_{mx}, u_{my} and u_{mz}. Detailed formulae are provided in the Appendix.

For the 3D curvilinear coordinates case, the nonsingular mapping is: $x = x(\xi, \eta, \zeta)$; $y = y(\xi, \eta, \zeta)$; $z = z(\xi, \eta, \zeta)$. The related Jacobian matrix and inverse matrix are:

$$\mathbf{J} = \frac{\partial(x, y, z)}{\partial(\xi, \eta, \zeta)} = \begin{pmatrix} x_\xi & x_\eta & x_\zeta \\ y_\xi & y_\eta & y_\zeta \\ z_\xi & z_\eta & z_\zeta \end{pmatrix} \quad \text{and} \quad \mathbf{J}^{-1} = \frac{\partial(\xi, \eta, \zeta)}{\partial(x, y, z)} = \begin{pmatrix} \xi_x & \xi_y & \xi_z \\ \eta_x & \eta_y & \eta_z \\ \zeta_x & \zeta_y & \zeta_z \end{pmatrix}.$$

The 3D ideal MHD equations in the computational domain are as follows:

$$\frac{\partial \widetilde{\mathbf{U}}}{\partial t} + \frac{\partial \widetilde{\mathbf{F}}}{\partial \xi} + \frac{\partial \widetilde{\mathbf{G}}}{\partial \eta} + \frac{\partial \widetilde{\mathbf{H}}}{\partial \zeta} = 0,$$

where

$$\begin{aligned} \widetilde{\mathbf{U}} &= J\mathbf{U}, \\ \widetilde{\mathbf{F}} &= J\xi_x\mathbf{F} + J\xi_y\mathbf{G} + J\xi_z\mathbf{H}, \\ \widetilde{\mathbf{G}} &= J\eta_x\mathbf{F} + J\eta_y\mathbf{G} + J\eta_z\mathbf{H}, \\ \widetilde{\mathbf{H}} &= J\zeta_x\mathbf{F} + J\zeta_y\mathbf{G} + J\zeta_z\mathbf{H}. \end{aligned}$$

The relationships of conservative variables and flux vectors as well as their corresponding spatial derivatives in the physical domain and computational domain for the 3D case are as follows:

$$\begin{aligned} \widetilde{\mathbf{U}}_\phi &= J_\phi\mathbf{U} + J\mathbf{U}_\phi, \\ \widetilde{\mathbf{F}}_\phi &= (J\xi_x)_\phi\mathbf{F} + (J\xi_y)_\phi\mathbf{G} + (J\xi_z)_\phi\mathbf{H} + J\xi_x\mathbf{F}_\phi + J\xi_y\mathbf{G}_\phi + J\xi_z\mathbf{H}_\phi, \\ \widetilde{\mathbf{G}}_\phi &= (J\eta_x)_\phi\mathbf{F} + (J\eta_y)_\phi\mathbf{G} + (J\eta_z)_\phi\mathbf{H} + J\eta_x\mathbf{F}_\phi + J\eta_y\mathbf{G}_\phi + J\eta_z\mathbf{H}_\phi, \\ \widetilde{\mathbf{H}}_\phi &= (J\zeta_x)_\phi\mathbf{F} + (J\zeta_y)_\phi\mathbf{G} + (J\zeta_z)_\phi\mathbf{H} + J\zeta_x\mathbf{F}_\phi + J\zeta_y\mathbf{G}_\phi + J\zeta_z\mathbf{H}_\phi, \\ \mathbf{U}_\phi &= \mathbf{U}_x x_\phi + \mathbf{U}_y y_\phi + \mathbf{U}_z z_\phi, \\ \mathbf{F}_\phi &= \frac{\partial \mathbf{F}}{\partial \mathbf{U}}\mathbf{U}_\phi, \qquad \mathbf{G}_\phi = \frac{\partial \mathbf{G}}{\partial \mathbf{U}}\mathbf{U}_\phi, \end{aligned}$$

where the subscript "ϕ" denotes ξ, η or ζ.

4. Method to clean the magnetic divergence error

When using Eqs. (4)–(7) to get the first-order derivatives relative to B_x, B_y, we find this is a set of over-determined equations, so we use the least-squares method to solve it. Then the magnetic field divergence-free condition:

$$\nabla \cdot \mathbf{B} = \frac{\partial B_x}{\partial x} + \frac{\partial B_y}{\partial y} = u_{6x} + u_{7y} = 0, \tag{22}$$

can be combined with other equations relative to B_x and B_y to obtain a new set of over-determined equations. Thus, by using the least-squares method, the magnetic field divergence can be fundamentally controlled. The details of this method you can refer Yang et al. [52]. And you can also refer Balsara et al. [53]. In that paper they have given a discussion in detail about how to design schemes to preserve divergence-free combined with the magnetic field divergence-free constraint condition, i.e., "$\nabla \cdot \mathbf{B} = 0$".

For the 3D case, when using Eqs. (A.1)–(A.8) to get the first-order derivatives relative to B_x, B_y, B_z, we use the least-squares method to solve it, and the magnetic field divergence-free condition is:

$$\nabla \cdot \mathbf{B} = \frac{\partial B_x}{\partial x} + \frac{\partial B_y}{\partial y} + \frac{\partial B_z}{\partial z} = u_{6x} + u_{7y} + u_{8z} = 0. \tag{23}$$

We should note that when using general curvilinear coordinates, Eq. (22) and Eq. (23) are satisfied in the physical domain. However, in the computational domain, we need to use transformation to get the equivalent formula. Take Eq. (23) as an example. According to the chain rule, we obtain

$$\begin{aligned} \mathbf{U}_x &= \mathbf{U}_\xi\xi_x + \mathbf{U}_\eta\eta_x + \mathbf{U}_\zeta\zeta_x, \\ \mathbf{U}_y &= \mathbf{U}_\xi\xi_y + \mathbf{U}_\eta\eta_y + \mathbf{U}_\zeta\zeta_y, \\ \mathbf{U}_z &= \mathbf{U}_\xi\xi_z + \mathbf{U}_\eta\eta_z + \mathbf{U}_\zeta\zeta_z. \end{aligned}$$

Then combined with the relationships $\widetilde{\mathbf{U}}_\xi = J_\xi \mathbf{U} + J\mathbf{U}_\xi$, $\widetilde{\mathbf{U}}_\eta = J_\eta \mathbf{U} + J\mathbf{U}_\eta$, $\widetilde{\mathbf{U}}_\zeta = J_\zeta \mathbf{U} + J\mathbf{U}_\zeta$, we can obtain the equivalent formula of Eq. (23) in the computational domain is as follows:

$$\frac{\widetilde{u}_{6\xi} - J_\xi u_6}{J}\xi_x + \frac{\widetilde{u}_{6\eta} - J_\eta u_6}{J}\eta_x + \frac{\widetilde{u}_{6\zeta} - J_\zeta u_6}{J}\zeta_x + \frac{\widetilde{u}_{7\xi} - J_\xi u_7}{J}\xi_y + \frac{\widetilde{u}_{7\eta} - J_\eta u_7}{J}\eta_y + \frac{\widetilde{u}_{7\zeta} - J_\zeta u_7}{J}\zeta_y + \frac{\widetilde{u}_{8\xi} - J_\xi u_8}{J}\xi_z + \frac{\widetilde{u}_{8\eta} - J_\eta u_8}{J}\eta_z + \frac{\widetilde{u}_{8\zeta} - J_\zeta u_8}{J}\zeta_z = 0.$$

5. Numerical tests

In this section, we show the use of some benchmarks to demonstrate the excellent characteristics of the upwind CESE scheme in capturing discontinuities and maintaining accuracy in both rectangular and general curvilinear coordinates. All the CFL number used are 0.8.

5.1. MHD blast wave problem in both rectangular and general curvilinear coordinates for the 2D case

MHD blast wave problem was designed by Skinner and Ostriker [54]. In this, fast shocks are driven to move outward by an over-pressured region. Then the fast shocks compress the plasma and magnetic field ahead while the plasma behind will become rarefied.

Firstly, we test the MHD blast wave problem in both rectangular coordinates and general curvilinear ordinates for the 2D case.

Similar to that in Ref. [54], the computational domain in rectangular coordinates is $(x, y) \in [1, 2] \times [-0.5, 0.5]$ and in polar coordinates is given as $(r, \theta) \in [1, 2] \times [-\frac{1}{3}, \frac{1}{3}]$, and the relationships between the computational domain (ξ, η) and the physical domain (x, y) are: $x = r\cos\theta$, $y = r\sin\theta$, where $r = e^\xi$, $\theta = \eta$. The initial conditions are given as follows:

$$\rho = 1, \quad v_x = v_y = v_z = 0, \quad B_x = B_y = 1/\sqrt{2}, \quad B_z = 0, \quad p = \begin{cases} 10 & \text{if} \sqrt{(x-1.5)^2 + y^2} < 0.1, \\ 0.1 & \text{otherwise.} \end{cases}$$

The boundary values are fixed.

5.2. MHD blast wave problem both in both rectangular and general curvilinear coordinates for the 3D case

Then we test the upwind CESE scheme in both rectangular coordinates and spherical coordinates for 3D MHD blast wave problem. The computational domain in rectangular coordinates is $(x, y, z) \in [1, 2] \times [-0.5, 0.5] \times [-0.5, 0.5]$ and the spherical coordinates is given as $(r, \theta, \phi) \in [1, 2] \times [\pi/2 - 1/3, \pi/2 + 1/3] \times [-1/3, 1/3]$. The relationship between the computational domain (ξ, η, ζ) and the physical domain (x, y, z) is: $x = r\sin\theta\cos\phi$, $y = r\sin\theta\sin\phi$, $z = r\cos\theta$, where $r = e^\xi$, $\theta = \eta$, $\phi = \zeta$. The initial conditions are given as follows:

$$\rho = 1, \quad v_x = v_y = v_z = 0, \quad B_x = B_y = B_z = 1/\sqrt{3}, \quad p = \begin{cases} 10 & \text{if} \sqrt{(x-1.5)^2 + y^2 + z^2} < 0.1, \\ 0.1 & \text{otherwise.} \end{cases}$$

The boundary values are fixed.

Fig. 4 and Fig. 5 give the contours of the density, pressure, specific kinetic energy and magnetic energy for the 2D MHD blast wave with 256×256 grids in rectangular coordinates at $t = 0.2$ by using original and upwind CESE schemes, respectively. Fig. 6 and Fig. 7 are the corresponding cases in curvilinear coordinates. From these plots, we can see that the structures are much clearer and identified by using upwind CESE scheme in both rectangular and curvilinear coordinates. From Fig. 8 to Fig. 11 which show the plots of the density, pressure, specific kinetic energy, and magnetic energy along line through the center ($y = 0$) of the 2D blast wave at $t = 0.2$ in curvilinear coordinates, we clearly observe that the discontinuous surfaces are much sharpener (such as those between $x = 1.25$ and $x = 1.35$, or $x = 1.65$ and $x = 1.75$). In addition, some small structures are captured very well by using the upwind CESE scheme while these discontinuous surfaces or small structures were smeared out more or less when using the original CESE scheme (especially at $x = 1.25$ or $x = 1.75$ in Fig. 8 and Fig. 9, between $x = 1.2$ and $x = 1.3$, between $x = 1.4$ and $x = 1.5$ or between $x = 1.5$ and $x = 1.6$, between $x = 1.7$ and $x = 1.8$ in Fig. 10, between $x = 1.3$ and $x = 1.7$ in Fig. 11).

Fig. 12 and Fig. 13 give the contour plots of the density, pressure and magnetic energy at the slice planes namely $z = 0$ or $y = 0$ for the 3D MHD blast wave with $128 \times 128 \times 128$ grids at $t = 0.2$ in rectangular coordinates by using original and upwind CESE schemes, respectively. Fig. 14 and Fig. 15 are their corresponding cases in curvilinear coordinates. Fig. 16 shows the pressures along lines through the center of the 3D blast wave namely $y = 0$, $z = 0$. From these figures, we can see that the upwind CESE scheme has similar remarkable advantages over the original CESE scheme as the 2D case when used in the 3D MHD irrespective of the type of coordinates. We used the Intel Fortran compiler running on the Intel Xeon E7450 with a CPU clock speed of 2.4 GHz, and using O4 optimization option. By testing the CPU time, we conclude that it consumes almost similar time as the original second-order CESE scheme and delivers much better results than it.

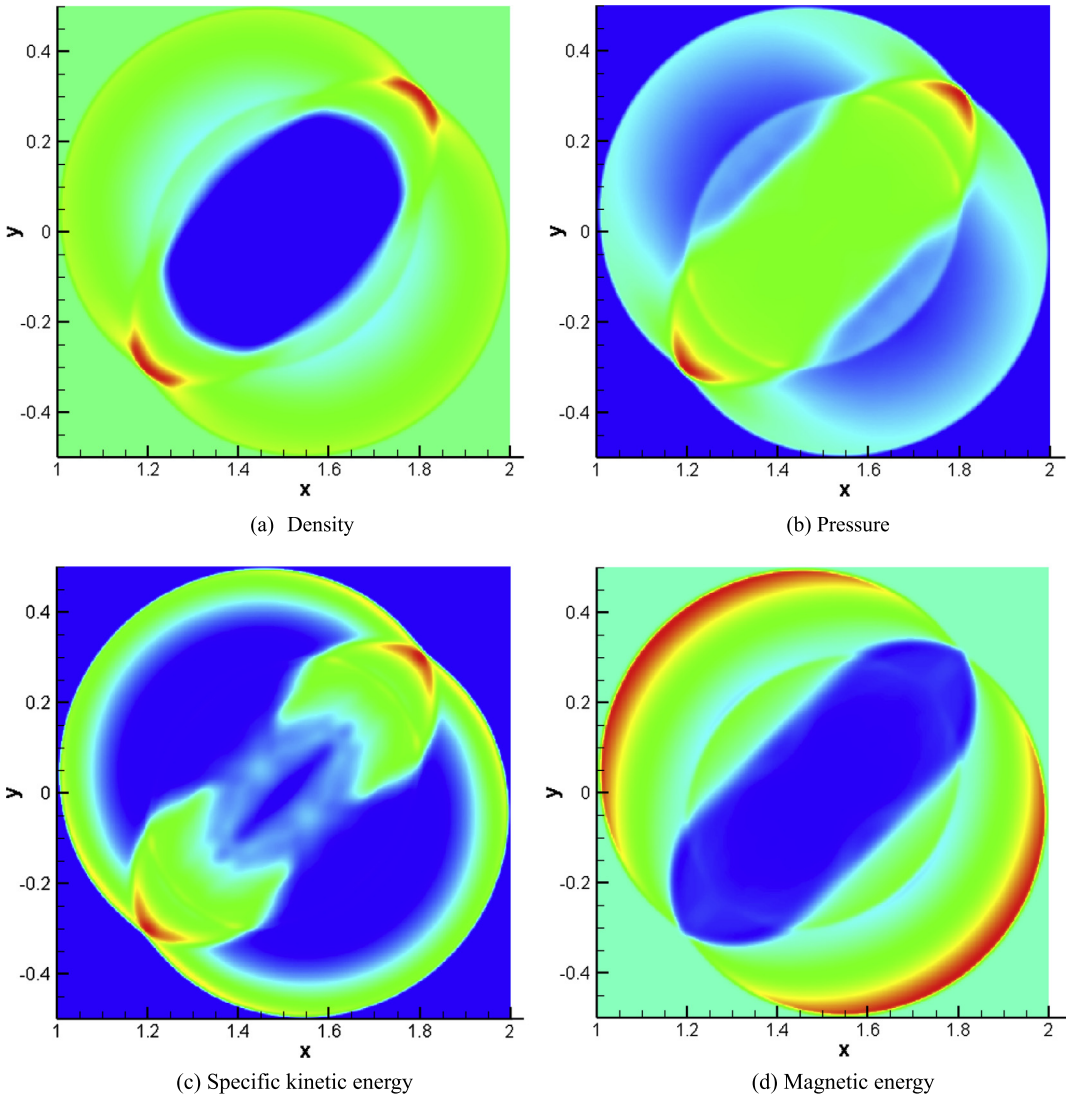

Fig. 4. Contours of the density, pressure, specific kinetic energy and magnetic energy at $t = 0.2$ for the 2D MHD blast wave in rectangular coordinates by using the original CESE scheme. (For the color versions of all the figures, the reader is referred to the web version of this article.)

6. Conclusions

In this study, we extended the upwind CESE scheme in rectangular coordinates to general curvilinear coordinates for both 2D and 3D MHD numerical simulations. In the future, this can be applied into the solar-terrestrial space physics problems, such as coronal mass ejections, the global evolution of magnetic structures, and solar wind and its interactions with the earth's atmosphere. This upwind CESE scheme also paves the way to achieve the perfect combination of the CESE and FVM and is very flexible, allowing to combine all kinds of upwind schemes for different problems. Although in this study we have used only the CESE + HLL, but it has shown remarkable advantages over the original CESE in capturing discontinuities and maintaining robust property has shown at no extra computational cost.

Acknowledgements

This work is jointly supported by the National Basic Research Program of China (Grant No. 2012CB825601), the National Natural Science Foundation of China (Grant Nos. 41231068, 41504132, 41274192, and 41531073), the Knowledge Innovation Program of the Chinese Academy of Sciences (Grant No. KZZD-EW-01-4), and the Specialized Research Fund for State Key Laboratories.

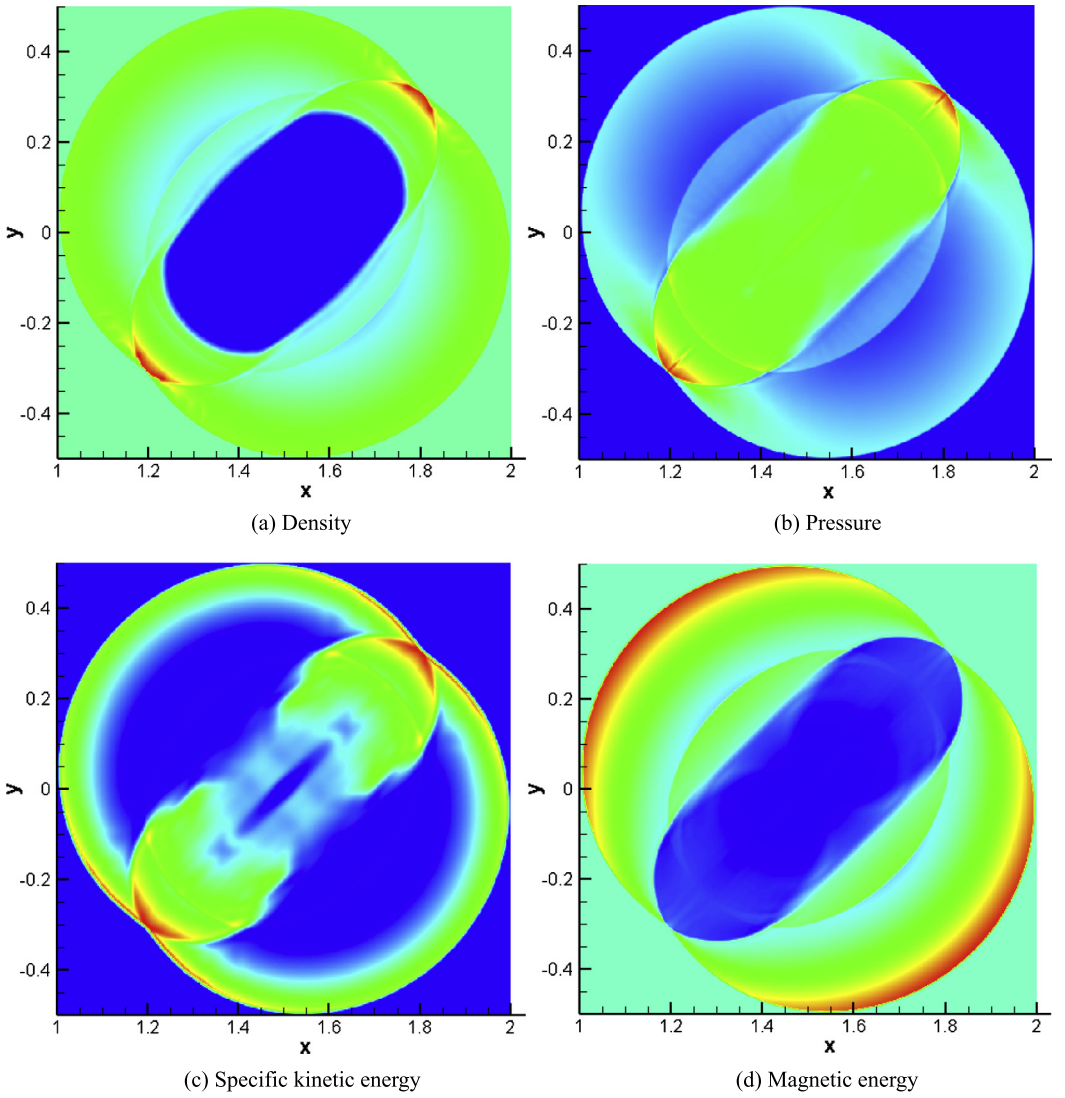

(a) Density (b) Pressure

(c) Specific kinetic energy (d) Magnetic energy

Fig. 5. Contours of the density, pressure, specific kinetic energy and magnetic energy at $t = 0.2$ for the 2D MHD blast wave in rectangular coordinates by using the upwind scheme.

Appendix A. Solving the derivations for 3D case by using upwind CESE scheme

Imposing conservation law, i.e., Eq. (3) on each sub-CE, we get

$$U_1^*(C_1^*)\frac{\Delta x\Delta y\Delta z}{8} = \left[u_m(C_1^*) - u_{mx}(C_1^*)\frac{\Delta x}{4} - u_{my}(C_1^*)\frac{\Delta y}{4} - u_{mz}(C_1^*)\frac{\Delta z}{4}\right]\frac{\Delta x\Delta y\Delta z}{8}$$
$$= U_1\frac{\Delta x\Delta y\Delta z}{8} + (F_1 - F_{1C})\frac{\Delta y\Delta z\Delta t}{8} + (G_1 - G_{1C})\frac{\Delta x\Delta z\Delta t}{8} + (H_1 - H_{1C})\frac{\Delta x\Delta y\Delta t}{8}, \quad \text{(A.1)}$$

$$U_2^*(C_1^*)\frac{\Delta x\Delta y\Delta z}{8} = \left[u_m(C_1^*) + u_{mx}(C_1^*)\frac{\Delta x}{4} - u_{my}(C_1^*)\frac{\Delta y}{4} - u_{mz}(C_1^*)\frac{\Delta z}{4}\right]\frac{\Delta x\Delta y\Delta z}{8}$$
$$= U_2\frac{\Delta x\Delta y\Delta z}{8} + (F_{1C} - F_2)\frac{\Delta y\Delta z\Delta t}{8} + (G_2 - G_{2C})\frac{\Delta x\Delta z\Delta t}{8} + (H_2 - H_{2C})\frac{\Delta x\Delta y\Delta t}{8}, \quad \text{(A.2)}$$

$$U_3^*(C_1^*)\frac{\Delta x\Delta y\Delta z}{8} = \left[u_m(C_1^*) + u_{mx}(C_1^*)\frac{\Delta x}{4} + u_{my}(C_1^*)\frac{\Delta y}{4} - u_{mz}(C_1^*)\frac{\Delta z}{4}\right]\frac{\Delta x\Delta y\Delta z}{8}$$
$$= U_3\frac{\Delta x\Delta y\Delta z}{8} + (F_{4C} - F_3)\frac{\Delta y\Delta z\Delta t}{8} + (G_{2C} - G_3)\frac{\Delta x\Delta z\Delta t}{8} + (H_3 - H_{3C})\frac{\Delta x\Delta y\Delta t}{8}, \quad \text{(A.3)}$$

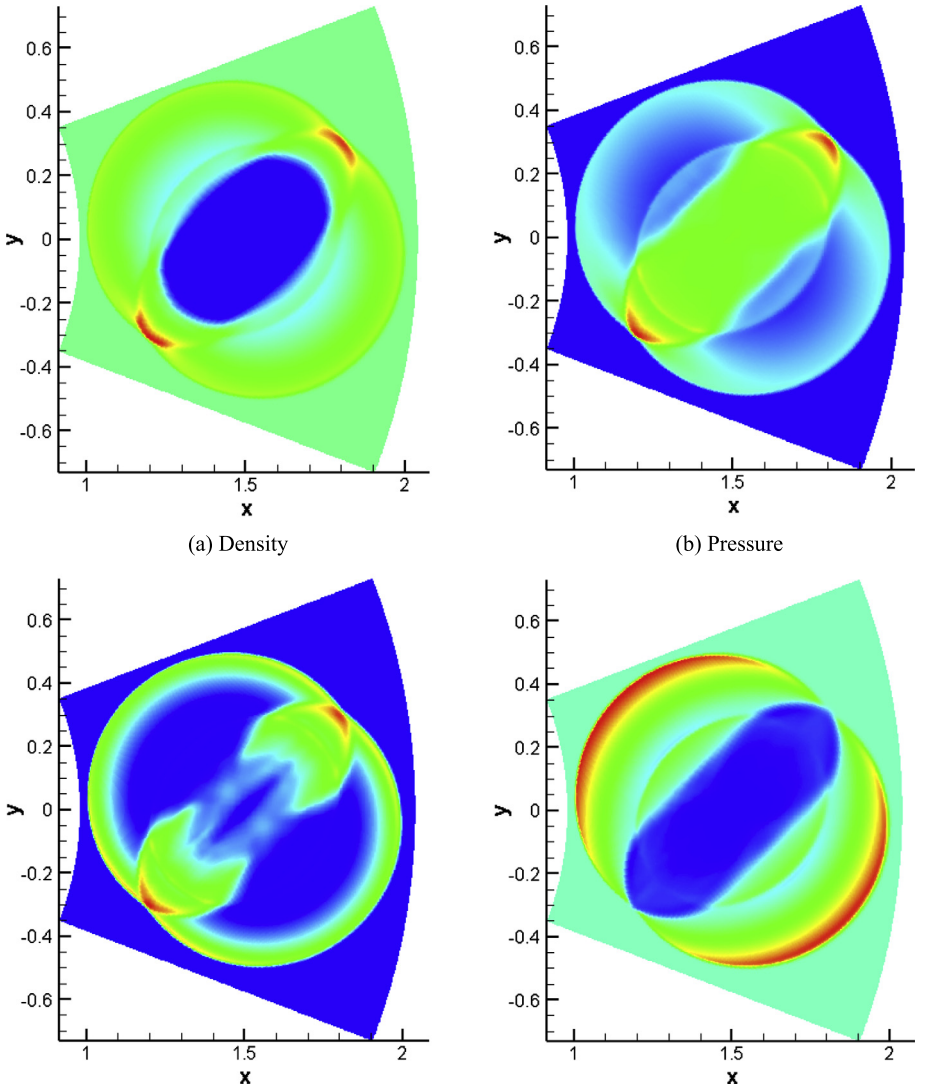

(a) Density (b) Pressure

(c) Specific kinetic energy (d) Magnetic energy

Fig. 6. Contours of the density, pressure, specific kinetic energy and magnetic energy at $t = 0.2$ for the 2D MHD blast wave in curvilinear coordinates by using the original CESE scheme.

$$U_4^*(C_1^*)\frac{\Delta x\Delta y\Delta z}{8} = \left[u_m(C_1^*) - u_{mx}(C_1^*)\frac{\Delta x}{4} + u_{my}(C_1^*)\frac{\Delta y}{4} - u_{mz}(C_1^*)\frac{\Delta z}{4}\right]\frac{\Delta x\Delta y\Delta z}{8}$$
$$= U_4\frac{\Delta x\Delta y\Delta z}{8} + (F_4 - F_{4C})\frac{\Delta y\Delta z\Delta t}{8} + (G_{1C} - G_4)\frac{\Delta x\Delta z\Delta t}{8} + (H_4 - H_{4C})\frac{\Delta x\Delta y\Delta t}{8}, \quad \text{(A.4)}$$

$$U_5^*(C_1^*)\frac{\Delta x\Delta y\Delta z}{8} = \left[u_m(C_1^*) - u_{mx}(C_1^*)\frac{\Delta x}{4} - u_{my}(C_1^*)\frac{\Delta y}{4} + u_{mz}(C_1^*)\frac{\Delta z}{4}\right]\frac{\Delta x\Delta y\Delta z}{8}$$
$$= U_5\frac{\Delta x\Delta y\Delta z}{8} + (F_5 - F_{2C})\frac{\Delta y\Delta z\Delta t}{8} + (G_5 - G_{4C})\frac{\Delta x\Delta z\Delta t}{8} + (H_{1C} - H_5)\frac{\Delta x\Delta y\Delta t}{8}, \quad \text{(A.5)}$$

$$U_6^*(C_1^*)\frac{\Delta x\Delta y\Delta z}{8} = \left[u_m(C_1^*) + u_{mx}(C_1^*)\frac{\Delta x}{4} - u_{my}(C_1^*)\frac{\Delta y}{4} + u_{mz}(C_1^*)\frac{\Delta z}{4}\right]\frac{\Delta x\Delta y\Delta z}{8}$$
$$= U_6\frac{\Delta x\Delta y\Delta z}{8} + (F_{2C} - F_6)\frac{\Delta y\Delta z\Delta t}{8} + (G_6 - G_{3C})\frac{\Delta x\Delta z\Delta t}{8} + (H_{2C} - H_6)\frac{\Delta x\Delta y\Delta t}{8}, \quad \text{(A.6)}$$

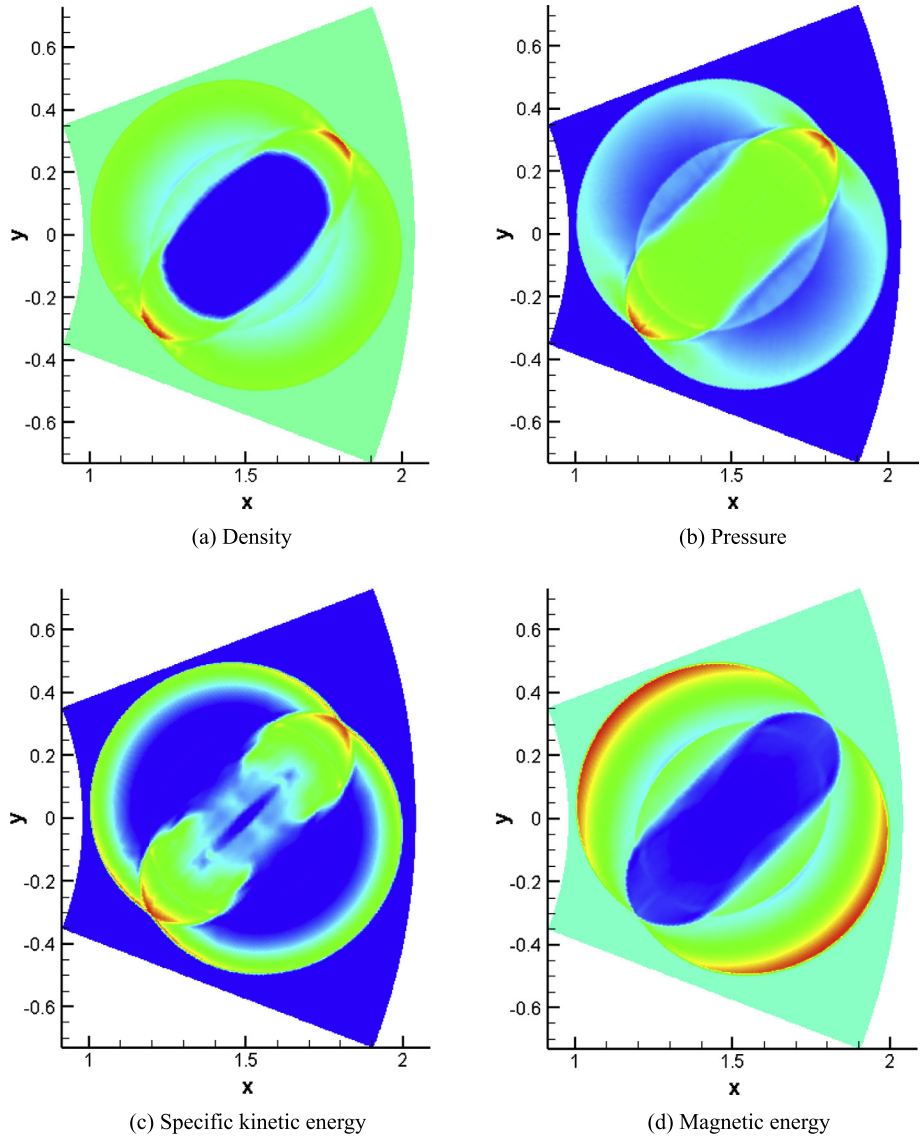

(a) Density (b) Pressure

(c) Specific kinetic energy (d) Magnetic energy

Fig. 7. Contours of the density, pressure, specific kinetic energy and magnetic energy at $t = 0.2$ for the 2D MHD blast wave in curvilinear coordinates by using the upwind CESE scheme.

$$U_7^*(C_1^*)\frac{\Delta x\Delta y\Delta z}{8} = \left[u_m(C_1^*) + u_{mx}(C_1^*)\frac{\Delta x}{4} + u_{my}(C_1^*)\frac{\Delta y}{4} + u_{mz}(C_1^*)\frac{\Delta z}{4}\right]\frac{\Delta x\Delta y\Delta z}{8}$$
$$= U_7\frac{\Delta x\Delta y\Delta z}{8} + (F_{3C} - F_7)\frac{\Delta y\Delta z\Delta t}{8} + (G_{3C} - G_7)\frac{\Delta x\Delta z\Delta t}{8} + (H_{3C} - H_7)\frac{\Delta x\Delta y\Delta t}{8}, \quad \text{(A.7)}$$

$$U_8^*(C_1^*)\frac{\Delta x\Delta y\Delta z}{8} = \left[u_m(C_1^*) - u_{mx}(C_1^*)\frac{\Delta x}{4} + u_{my}(C_1^*)\frac{\Delta y}{4} + u_{mz}(C_1^*)\frac{\Delta z}{4}\right]\frac{\Delta x\Delta y\Delta z}{8}$$
$$= U_8\frac{\Delta x\Delta y\Delta z}{8} + (F_8 - F_{3C})\frac{\Delta y\Delta z\Delta t}{8} + (G_{4C} - G_8)\frac{\Delta x\Delta z\Delta t}{8} + (H_{4C} - H_8)\frac{\Delta x\Delta y\Delta t}{8}. \quad \text{(A.8)}$$

Subtracting Eq. (A.1) from Eq. (A.2), subtracting Eq. (A.4) from Eq. (A.3), subtracting Eq. (A.5) from Eq. (A.6) and subtracting Eq. (A.8) from Eq. (A.7), we can obtain four groups of u_{mx} as follows:

$$u_{mx}(C_1^*) = \frac{2}{\Delta x}\left[(U_2 - U_1) + \frac{\Delta t}{\Delta x}(2F_{1C} - F_1 - F_2) + \frac{\Delta t}{\Delta y}(G_2 - G_1 + G_{1C} - G_{2C}) + \frac{\Delta t}{\Delta z}(H_2 - H_1 + H_{1C} - H_{2C})\right], \quad \text{(A.9)}$$

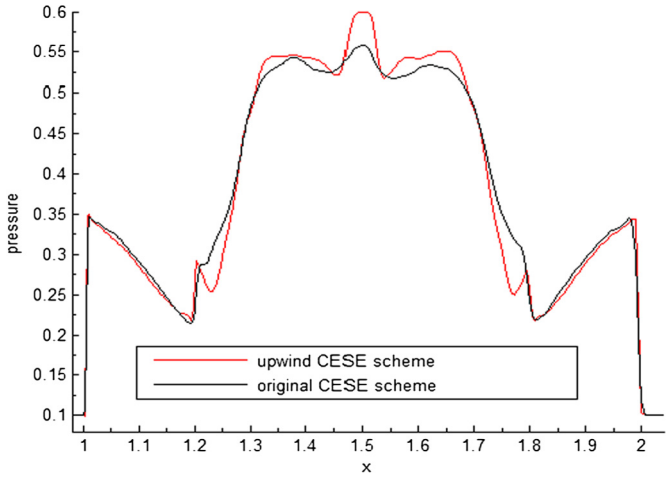

Fig. 8. Pressure along line through the center ($y = 0$) of the blast wave at $t = 0.2$ in curvilinear coordinates.

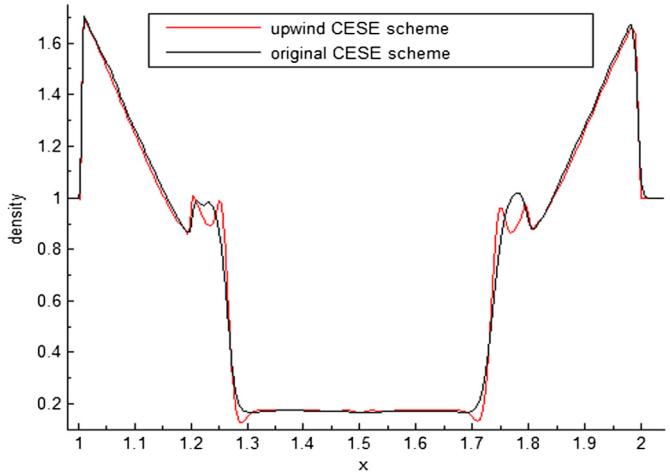

Fig. 9. Density along line through the center ($y = 0$) of the blast wave at $t = 0.2$ in curvilinear coordinates.

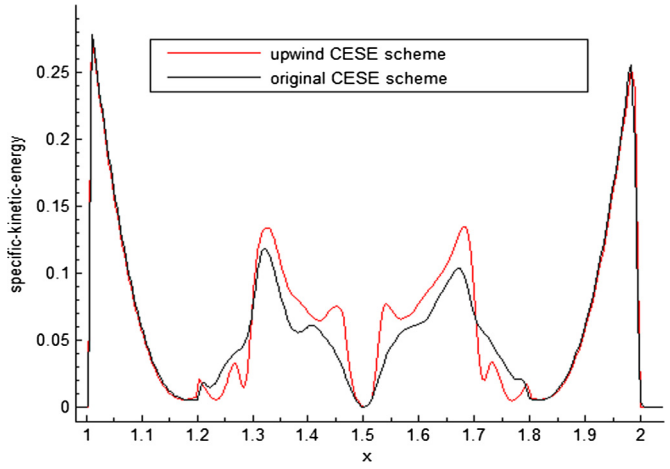

Fig. 10. Specific kinetic energy along line through the center ($y = 0$) of the blast wave at $t = 0.2$ in curvilinear coordinates.

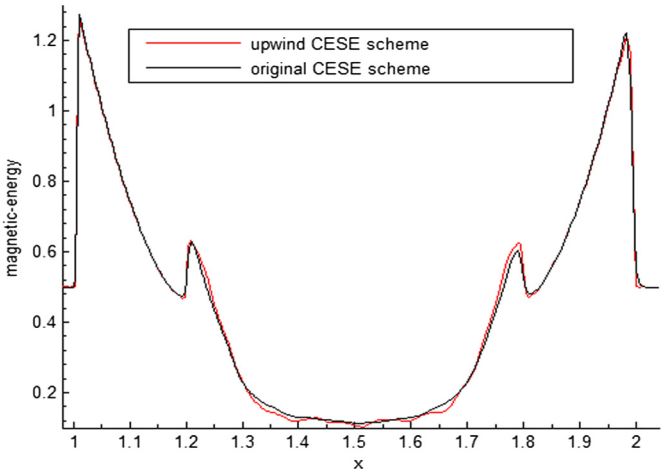

Fig. 11. Magnetic energy along line through the center ($y = 0$) of the blast wave at $t = 0.2$ in curvilinear coordinates.

$$u_{mx}(C_1^*) = \frac{2}{\Delta x}\left[(U_3 - U_4) + \frac{\Delta t}{\Delta x}(2F_{4C} - F_3 - F_4) + \frac{\Delta t}{\Delta y}(G_4 - G_3 + G_{2C} - G_{1C}) + \frac{\Delta t}{\Delta z}(H_3 - H_4 + H_{4C} - H_{3C})\right], \tag{A.10}$$

$$u_{mx}(C_1^*) = \frac{2}{\Delta x}\left[(U_6 - U_5) + \frac{\Delta t}{\Delta x}(2F_{2C} - F_5 - F_6) + \frac{\Delta t}{\Delta y}(G_6 - G_5 + G_{4C} - G_{3C}) + \frac{\Delta t}{\Delta z}(H_5 - H_6 + H_{2C} - H_{1C})\right], \tag{A.11}$$

$$u_{mx}(C_1^*) = \frac{2}{\Delta x}\left[(U_7 - U_8) + \frac{\Delta t}{\Delta x}(2F_{3C} - F_7 - F_8) + \frac{\Delta t}{\Delta y}(G_8 - G_7 + G_{3C} - G_{4C}) + \frac{\Delta t}{\Delta z}(H_8 - H_7 + H_{3C} - H_{4C})\right]. \tag{A.12}$$

In the similar way, we can get four groups of u_{my} and u_{mz}, respectively as follows:

$$u_{my}(C_1^*) = \frac{2}{\Delta y}\left[(U_3 - U_2) + \frac{\Delta t}{\Delta x}(F_2 - F_3 + F_{4C} - F_{1C}) + \frac{\Delta t}{\Delta y}(2G_{2C} - G_2 - G_3) + \frac{\Delta t}{\Delta z}(H_3 - H_2 + H_{2C} - H_{3C})\right], \tag{A.13}$$

$$u_{my}(C_1^*) = \frac{2}{\Delta y}\left[(U_4 - U_1) + \frac{\Delta t}{\Delta x}(F_4 - F_1 + F_{1C} - F_{4C}) + \frac{\Delta t}{\Delta y}(2G_{1C} - G_1 - G_4) + \frac{\Delta t}{\Delta z}(H_4 - H_1 + H_{1C} - H_{4C})\right], \tag{A.14}$$

$$u_{my}(C_1^*) = \frac{2}{\Delta y}\left[(U_7 - U_6) + \frac{\Delta t}{\Delta x}(F_6 - F_7 + F_{3C} - F_{2C}) + \frac{\Delta t}{\Delta y}(2G_{3C} - G_6 - G_7) + \frac{\Delta t}{\Delta z}(H_6 - H_7 + H_{3C} - H_{2C})\right], \tag{A.15}$$

$$u_{my}(C_1^*) = \frac{2}{\Delta y}\left[(U_8 - U_5) + \frac{\Delta t}{\Delta x}(F_8 - F_5 + F_{2C} - F_{3C}) + \frac{\Delta t}{\Delta y}(2G_{4C} - G_5 - G_8) + \frac{\Delta t}{\Delta z}(H_5 - H_8 + H_{4C} - H_{1C})\right]. \tag{A.16}$$

$$u_{mz}(C_1^*) = \frac{2}{\Delta z}\left[(U_5 - U_1) + \frac{\Delta t}{\Delta x}(F_5 - F_1 + F_{1C} - F_{2C}) + \frac{\Delta t}{\Delta y}(G_5 - G_1 + G_{1C} - G_{4C}) + \frac{\Delta t}{\Delta z}(2H_{1C} - H_1 - H_5)\right], \tag{A.17}$$

$$u_{mz}(C_1^*) = \frac{2}{\Delta z}\left[(U_6 - U_2) + \frac{\Delta t}{\Delta x}(F_2 - F_6 + F_{2C} - F_{1C}) + \frac{\Delta t}{\Delta y}(G_6 - G_2 + G_{2C} - G_{3C}) + \frac{\Delta t}{\Delta z}(2H_{2C} - H_2 - H_6)\right], \tag{A.18}$$

$$u_{mz}(C_1^*) = \frac{2}{\Delta z}\left[(U_7 - U_3) + \frac{\Delta t}{\Delta x}(F_3 - F_7 + F_{3C} - F_{4C}) + \frac{\Delta t}{\Delta y}(G_3 - G_7 + G_{3C} - G_{2C}) + \frac{\Delta t}{\Delta z}(2H_{3C} - H_3 - H_7)\right], \tag{A.19}$$

$$u_{mz}(C_1^*) = \frac{2}{\Delta z}\left[(U_8 - U_4) + \frac{\Delta t}{\Delta x}(F_8 - F_4 + F_{4C} - F_{3C}) + \frac{\Delta t}{\Delta y}(G_4 - G_8 + G_{4C} - G_{1C}) + \frac{\Delta t}{\Delta z}(2H_{4C} - H_8 - H_4)\right]. \tag{A.20}$$

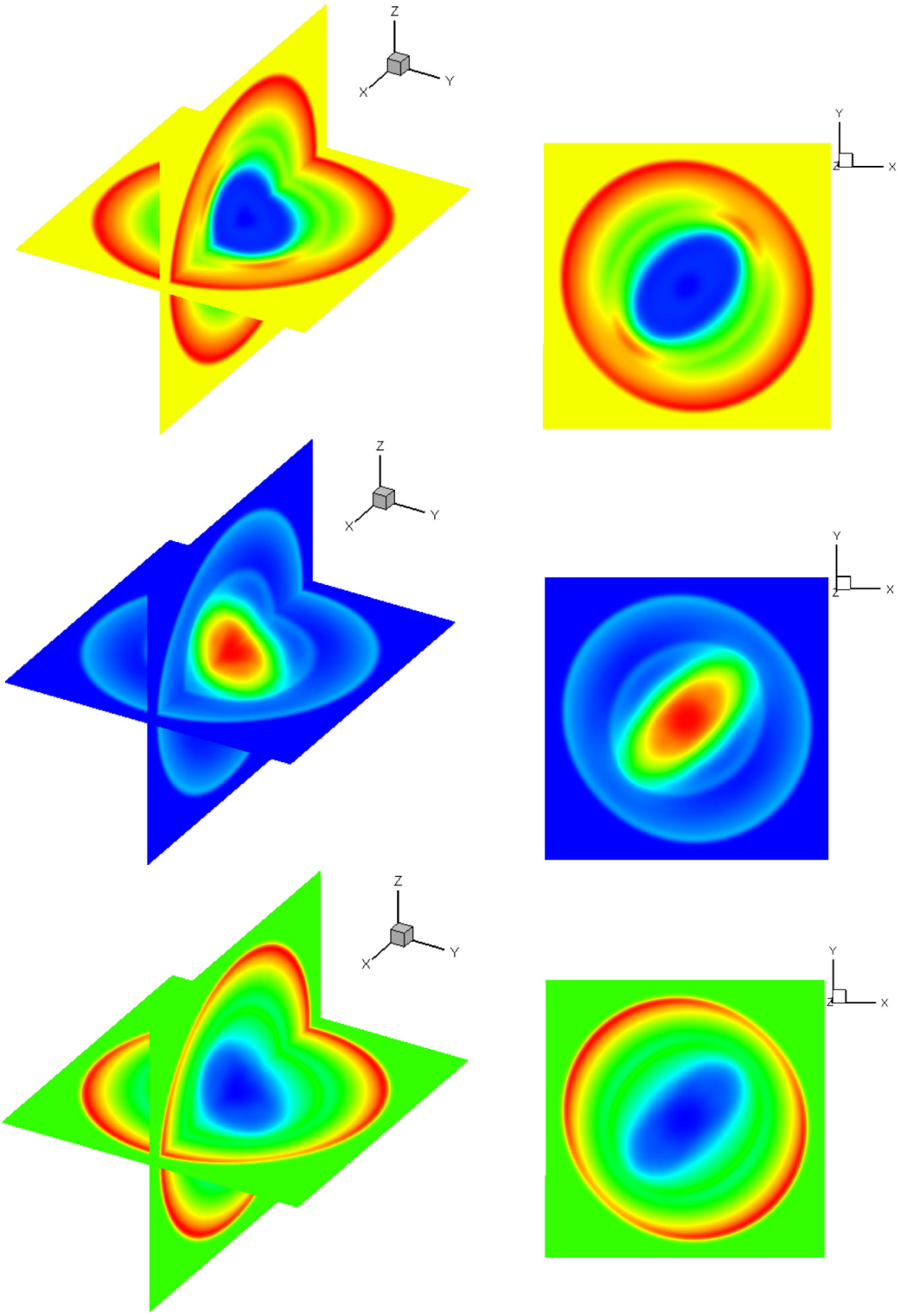

Fig. 12. Contours of the density, pressure and magnetic energy at the slice planes namely $z = 0$ and $y = 0$ for the 3D MHD blast wave at $t = 0.2$ in rectangular coordinates by using the original CESE scheme.

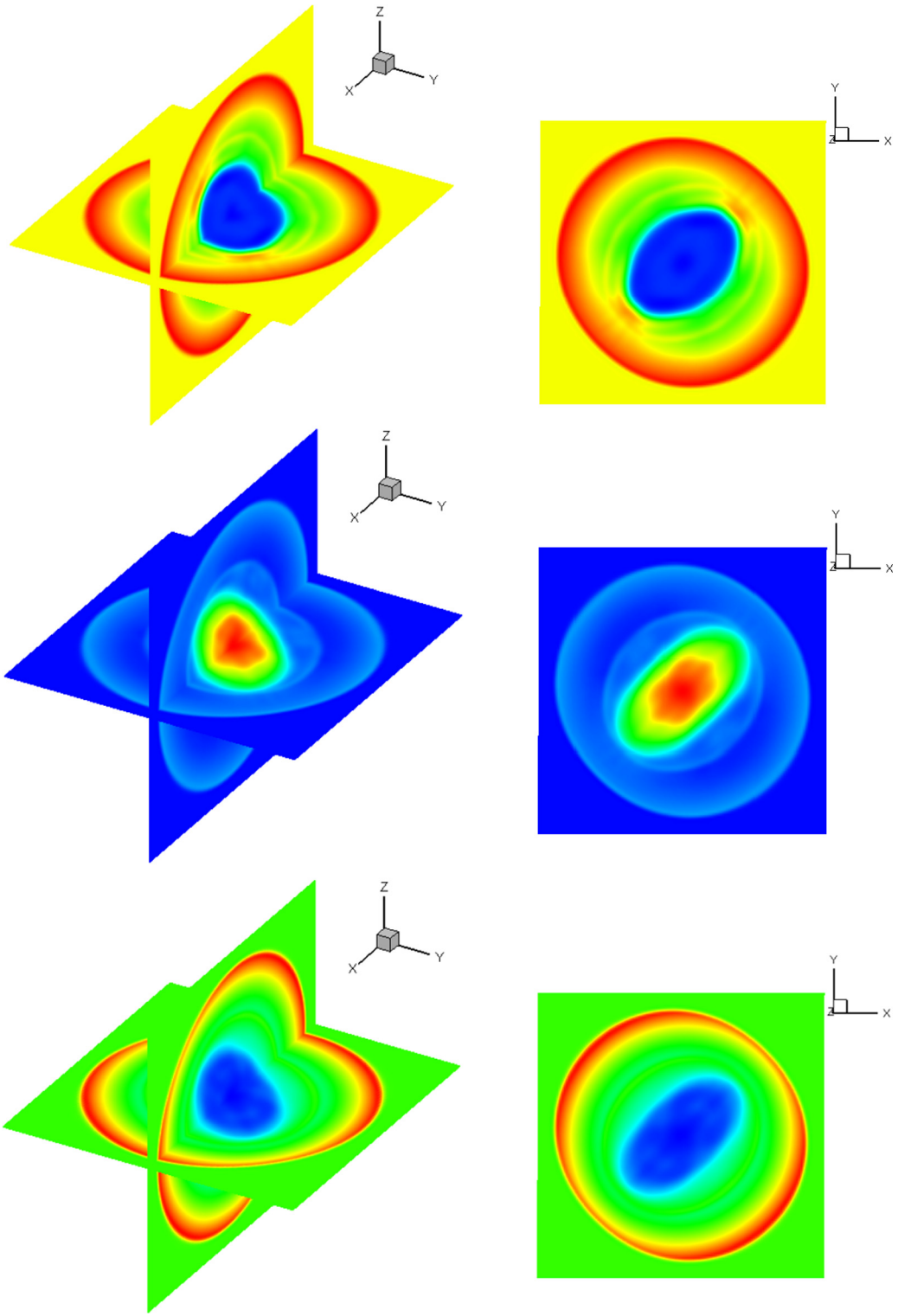

Fig. 13. Contours of the density, pressure and magnetic energy at the slice planes namely $z = 0$ and $y = 0$ for the 3D MHD blast wave at $t = 0.2$ in rectangular coordinates by using the upwind CESE scheme.

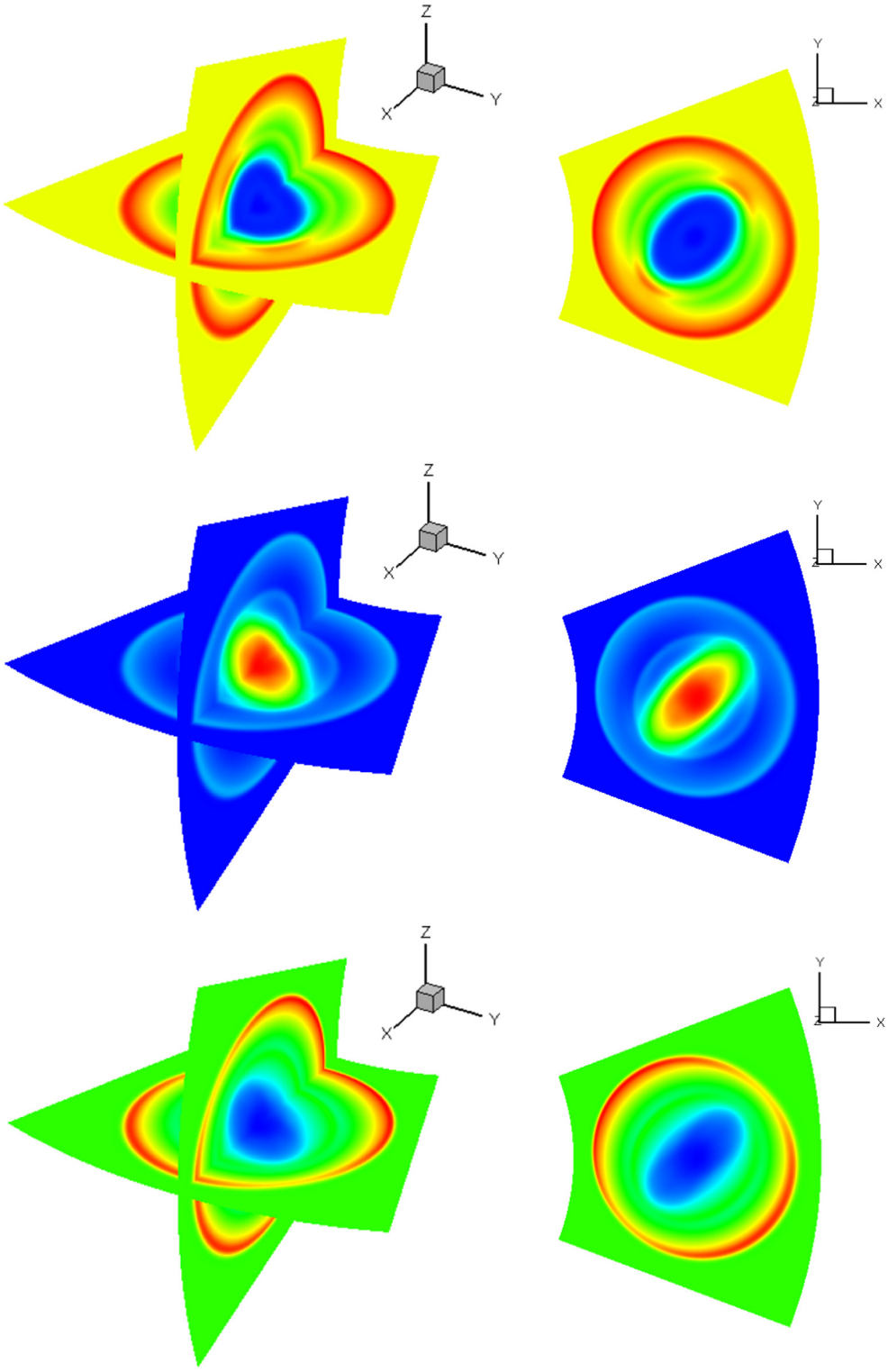

Fig. 14. Contours of the density, pressure and magnetic energy at the slice planes namely $z = 0$ and $y = 0$ for the 3D MHD blast wave at $t = 0.2$ in curvilinear coordinates by using the original CESE scheme.

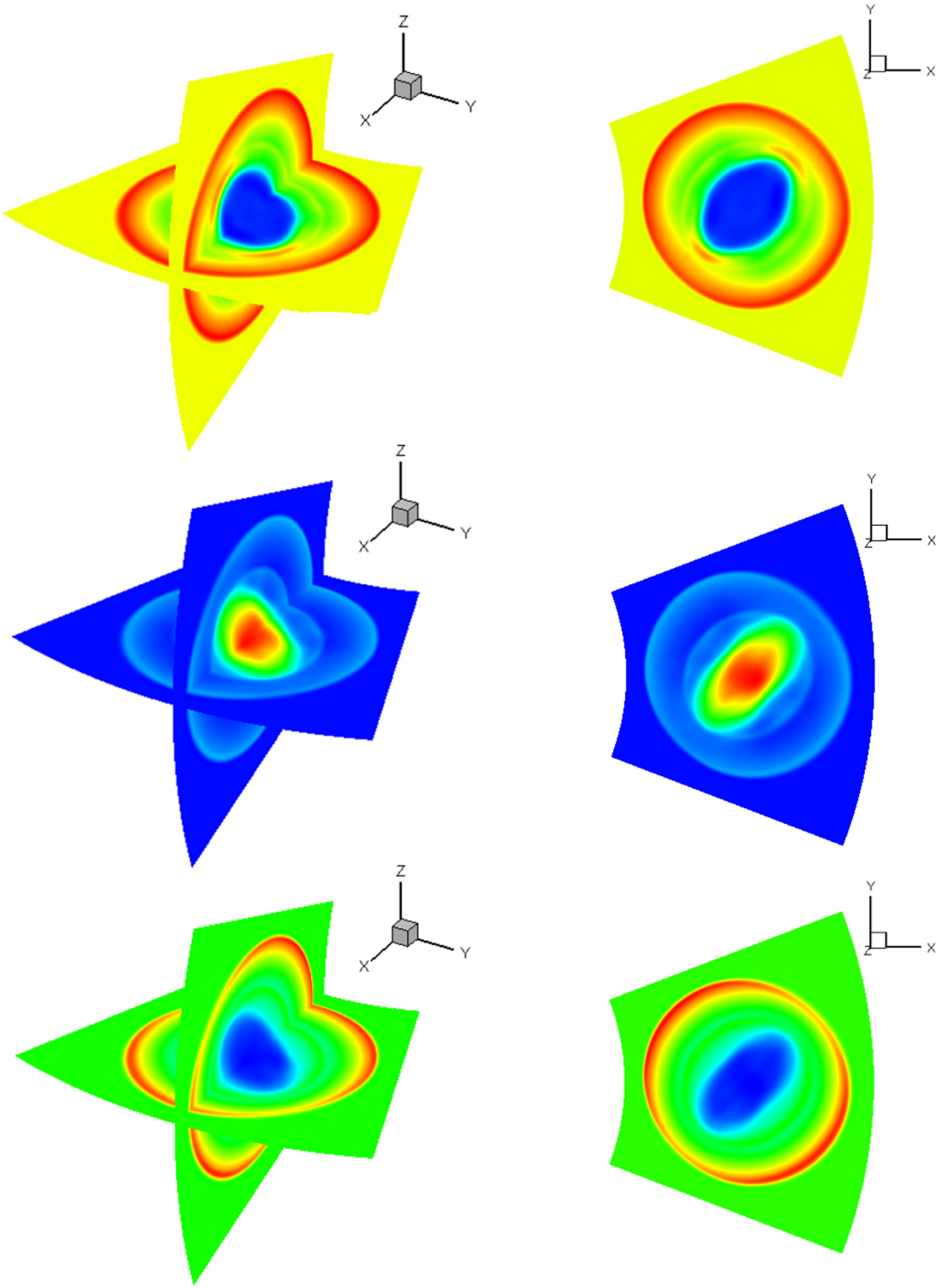

Fig. 15. Contours of the density, pressure and magnetic energy at the slice planes namely $z = 0$ and $y = 0$ for the 3D MHD blast wave at $t = 0.2$ in curvilinear coordinates by using the upwind CESE scheme.

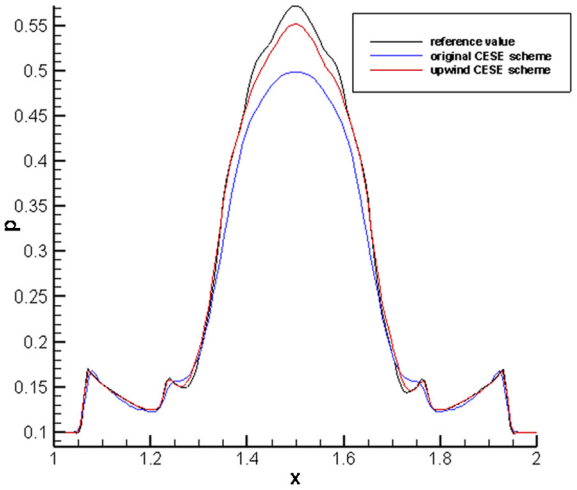

Fig. 16. Pressure line profile along the center of the 3D blast wave namely $y = 0$, $z = 0$ at $t = 0.2$ in curvilinear coordinates.

References

[1] H. Shen, C.Y. Wen, D.L. Zhang, A characteristic space-time conservation element and solution element method for conservation laws, J. Comput. Phys. 288 (2015) 101–118.
[2] H. Shen, C.Y. Wen, A characteristic space-time conservation element and solution element method for conservation laws II, J. Comput. Phys. 305 (2016) 775–792.
[3] S. Evje, T. Flatten, Hybrid flux-splitting schemes for a common two-fluid model, J. Comput. Phys. 192 (2003) 175–210.
[4] 计算流体力学讲义李新亮, 中科院力学所, www.cfluid.com or http://cid-1cc0dcbff560c149.skydrive.live.com/browse.aspx/.Public.
[5] M.S. Liou, C.J. Steffen, A new flux splitting scheme, J. Comput. Phys. 107 (1993) 23–39.
[6] M.S. Liou, A sequel to AUSM: AUSM+, J. Comput. Phys. 129 (1996) 364–382.
[7] A. Jameson, Analysis and design of numerical schemes for gas dynamics, I: artificial diffusion, upwind biasing, limiters and their effect on accuracy and multigrid convergence in transonic and hypersonic flow, J. Comput. Fluid Dyn. 4 (1995) 171–218.
[8] A. Jameson, Analysis and design of numerical schemes for gas dynamics, II: artificial diffusion and discrete shock structure, J. Comput. Fluid Dyn. 5 (1995) 1–38.
[9] G.C. Zha, E. Bilgen, Numerical solutions of Euler equations by using a new flux vector splitting scheme, Int. J. Numer. Methods Fluids 17 (1993) 115–144.
[10] G.C. Zha, Y.Q. Shen, B.Y. Wang, An improved low diffusion E-CUSP upwind scheme, Comput. Fluids 48 (2011) 214–220.
[11] Y.Q. Shen, G.C. Zha, M.A. Huerta, E-CUSP scheme for the equations of ideal magnetohydrodynamics with high order WENO scheme, J. Comput. Phys. 231 (2012) 6233–6247.
[12] J.R. Edwards, A low-diffusion flux-splitting scheme for Navier–Stokes calculations, Comput. Fluids 6 (1997) 635–659.
[13] M. Sun, K. Takayama, An artificially upstream flux vector splitting scheme for the Euler equations, J. Comput. Phys. 189 (2003) 305–329.
[14] J.L. Steger, R.F. Warming, Flux vector splitting of the inviscid gasdynamic equations with application to finite difference method, J. Comput. Phys. 40 (1981) 263–293.
[15] B. Li, L. Yuan, Convergence issue in using high-resolution schemes and lower-upper symmetric Gauss–Seidel method for steady shock-induced combustion problems, Int. J. Numer. Methods Fluids 71 (2013) 1422–1437.
[16] M.S. Liou, B. van Leer, J.S. Shuen, Splitting of inviscid fluxes for real gases, J. Comput. Phys. 87 (1990) 1–24.
[17] R.W. MacCormack, An Upwind Conservation form Method for Ideal Magnetohydrodynamics Equations, AIAA, 1999, Paper 99-3609.
[18] A. Harten, P.D. Lax, B. van Leer, On upstream differencing and Godunov-type schemes for hyperbolic conservation laws, SIAM Rev. 25 (1983) 35–61.
[19] D.S. Balsara, Multidimensional HLLE Riemann solver: application to Euler and magnetohydrodynamical flows, J. Comput. Phys. 229 (2010) 1970–1993.
[20] D.S. Balsara, M. Dumbser, R. Abgrall, Multidimensional HLL and HLLC Riemann solvers for unstructured meshes – with application to Euler and MHD flows, J. Comput. Phys. 261 (2014) 172–208.
[21] P. Janhunen, A positive conservative method for magnetohydrodynamics based on HLL and Roe methods, J. Comput. Phys. 160 (2000) 649–661.
[22] E.F. Toro, M. Spruce, W. Speares, Restoration of the contact surface in the HLL Riemann solver, Shock Waves 4 (1994) 25–34.
[23] E.F. Toro, Riemann Solvers and Numerical Methods for Fluid Dynamics, third edition, Springer, 2009.
[24] K.F. Gurski, An HLLC-type approximate Riemann solver for ideal magnetohydrodynamics, SIAM J. Sci. Comput. 25 (2004) 2165–2187.
[25] S.T. Li, An HLLC Riemann solver for magnetohydrodynamics, J. Comput. Phys. 203 (2005) 344–357.
[26] T. Miyoshi, K. Kusano, A multi-state HLL approximate Riemann solver for ideal magnetohydrodynamics, J. Comput. Phys. 208 (2005) 315–344.
[27] A. Mignone, M. Ugliano, G. Bodo, A five-wave Harten–Lax–van Leer Riemann solver for relativistic magnetohydrodynamics, Mon. Not. R. Astron. Soc. 393 (2009) 1141–1156.
[28] P.L. Roe, Approximate Riemann solvers, parameter vectors, and difference schemes, J. Comput. Phys. 43 (1981) 357–372.
[29] P. Cargo, G. Gallice, Roe matrices for ideal MHD and systematic construction of roe matrices for systems of conservation laws, J. Comput. Phys. 136 (1997) 446–466.
[30] D.S. Balsara, Total variation diminishing scheme for adiabatic and isothermal magnetohydrodynamics, Astrophys. J. Suppl. Ser. 116 (1998) 133–153.
[31] P.L. Roe, D.S. Balsara, Notes on the eigensystem of magnetohydrodynamics, SIAM J. Appl. Math. 56 (1996) 57–67.
[32] D.S. Balsara, Linearized formulation of the Riemann problem for adiabatic and isothermal magnetohydrodynamics, Astrophys. J. Suppl. Ser. 116 (1998) 119–131.
[33] G. Tchuen, F. Fogang, Y. Burtschell, P. Woafo, A hybrid numerical method and its application to inviscid compressible flow problems, Comput. Phys. Commun. 185 (2014) 479–488.
[34] F. Fogang, G. Tchuen, Y. Burtschell, P. Woafo, An extension of AUFSR scheme for the ideal magnetohydrodynamics equations, Comput. Fluids 114 (2015) 297–313.

[35] C.C. Rossow, A flux-splitting scheme for compressible and incompressible flows, J. Comput. Phys. 164 (2000) 104–122.
[36] F. Coquel, M.S. Liou, Hybrid Upwind Splitting (HUS) by a Field by Field Decomposition, ICOMP-95-2, NASA, 1995.
[37] K. Kitamura, T. Nonomura, Simple and robust HLLC extensions of two-fluid AUSM for multiphase flow computations, Comput. Fluids 100 (2014) 321–335.
[38] P.T. Kapen, T. Ghislain, A new flux splitting scheme based on Toro–Vazquez and HLL scheme for the Euler equations, J. Comput. Methods Phys. 2014 (2014).
[39] C.M. Xisto, J.C. P´ascoa, P.J. Oliveira, A pressure-based method with AUSM-type fluxes for MHD flows at arbitrary Mach numbers, Int. J. Numer. Methods Fluids 72 (2013) 1165–1182.
[40] C.M. Xisto, J.C. P´ascoa, P.J. Oliveira, D.A. Nicolini, A hybrid pressure-density-based algorithm for the Euler equations at all Mach number regimes, Int. J. Numer. Methods Fluids 70 (2012) 961–976.
[41] H. Nishikawa, K. Kitamura, Very simple, carbuncle-free, boundary-layer-resolving, rotated-hybrid Riemann solvers, J. Comput. Phys. 227 (2008) 2560–2581.
[42] Y.X. Ren, A robust shock-capturing scheme based on rotated Riemann solvers, Comput. Fluids 32 (2003) 1379–1403.
[43] D.W. Levy, K.G. Powell, B.V. Leer, Use of a rotated solver for the two-dimensional Euler equations, J. Comput. Phys. 106 (1993) 201–214.
[44] S.C. Chang, The method of space-time conservation element and solution element – a new approach for solving the Navier–Stokes and Euler equations, J. Comput. Phys. 119 (1995) 295–324.
[45] X.Y. Wang, A Summary of the Space-Time Conservation Element and Solution Element (CESE), Method, NASA/TM-2015-218743, 2015.
[46] H.T. Huynh, Analysis and Improvement of Upwind and Centered Schemes on Quadrilateral and Triangular Meshes, AIAA 2003-3541, 2003.
[47] M. Vinokur, Conservation equations of gas-dynamics in curvilinear coordinate systems, J. Comput. Phys. 14 (1974) 105–125.
[48] H. Viviand, Conservation Forms of Gas Dynamic Equations, European Space Research Organization Technical Translation, ESRO-TT-144, 1 1974, pp. 153–159.
[49] D. Bilyeu, A High-Order Conservation Element Solution Element Method for Solving Hyperbolic Differential Equations on Unstructured Grid, PhD Thesis, University of the Ohio State, 2014.
[50] Z.C. Zhang, S.T. John Yu, S.C. Chang, A space-time conservation element and solution element method for solving the two- and three-dimensional unsteady Euler equations using quadrilateral and hexahedral meshes, J. Comput. Phys. 175 (2002) 168–199.
[51] X.S. Feng, Y.Q. Hu, F.S. Wei, Modeling the resistive MHD by the CESE method, Sol. Phys. 235 (2006) 235–257.
[52] Y. Yang, X.S. Feng, C.W. Jiang, A high-order CESE scheme with a new divergence-free method for MHD numerical simulation, J. Comput. Phys. 349 (2017) 561–581.
[53] D.S. Balsara, M. Dumbser, Divergence-free MHD on unstructured meshes using high order finite volume schemes based on multidimensional Riemann solvers, J. Comput. Phys. 299 (2015) 687–715.
[54] M.A. Skinner, E.C. Ostriker, The Athena astrophysical magnetohydrodynamics code in cylindrical geometry, Astrophys. J. Suppl. Ser. 188 (2010) 290–311.